JOURNAL OF MATERIALS SCIENCE 10 (1975) 1029–1036

Structural and textural effects of TeO_2 added to MoO_3

J. C. J. BART*, A. MARZI, F. PIGNATARO, A. CASTELLAN, N. GIORDANO†
Montedison, Research Center, 20021 Bollate, Milano, Italy

Morphological and microstructural characterization of the MoO_3–TeO_2 system has shown interparticle cementation of MoO_3 agglomerates by Te_2MoO_7 and second phase deposition along the cleavage planes in MoO_3 crystallites. The main morphological parameters of the binary system reflect the behaviour of the liquidus curve in the phase diagram. The size and shape of the component grains in the solid were determined. The porosity of the grains diminishes with increasing mobility of the matter during activation. Intergranular embrittlement of the solid and brittle fracture of MoO_3 crystallites due to oxygen depletion during reduction were examined by optical microscopy. The results are discussed in relation to the use of the MoO_3–TeO_2 system in oxidation catalysis.

1. Introduction

The present study was undertaken to contribute to the knowledge of a multicomponent industrial catalyst for the ammoxidation of propylene, based partially on TeO_2 and MoO_3. Related investigations [1, 2] have provided detailed information about the phase relationships in the binary oxide system: chemical interaction has shown to lead to the formation of a new phase, Te_2MoO_7, influencing the sintering and crystallization process, as well as the physical properties.

In this paper we limit ourselves to the effects of the addition of TeO_2 on the morphological and microstructural properties of MoO_3. The phenomenology of interface formation at MoO_3 grain boundaries by interaction with TeO_2 is described and the influence of the second phase on the embrittlement of MoO_3 particles is indicated as a function of the composition. Structure and texture of MoO_3–Te_2MoO_7 aggregates were also investigated optically after etching with reducing agents. This study thus contributes to the general knowledge of textural modifications induced by chemical interactions and to the evaluation of the properties of Te–Mo based oxidation catalysts [3, 4].

2. Experimental

2.1. Sample preparation

As the same procedure was used for all binary oxide compositions, we report here the conditions for the preparation of the sample with molar ratio MoO_3:TeO_2 = 12:1. To 111 g $(NH_4)_6Mo_7O_{24}.4H_2O$ (Rudi Pont), dissolved in 150 ml hot water, are added 11.95 g H_6TeO_6 (Schuchardt) and 40 ml 65% HNO_3. The mixture, brought to dryness at 110°C (12 h), is subsequently activated at the desired temperature.

Other compositions were prepared by varying the calculated amount of solid reagents. The final compositions were checked by atomic absorption techniques and were always in accordance with the theoretical formulations. Depending upon activation and quenching conditions (partially) crystalline or amorphous samples were obtained.

Binary oxide compositions supported on microspheroidal SiO_2 (75%) were prepared, as described for the sample $3TeO_2.12MoO_3$. A solution of 19.2 g $(NH_4)_6Mo_7O_{24}.4H_2O$ in 6.4 ml H_2O and 6.4 ml H_2O_2 is added to 6.12 g H_6TeO_6 dissolved in 25 ml H_2O and 10 g 65% HNO_3. After impregnation of 64.3 g SiO_2 (Ketjen) the resulting mass is brought to dryness

*Present address: Montedison Corporate Research Laboratories, Novara.
†Present address: Montedison Research Laboratories, Priolo, Sicily.

at 110°C for 4 h and is activated in air at 500°C for 8 h.

Reference will be made to the various samples by the atomic ratio Mo_xTe_y, labelled A (amorphous) or C (crystalline), according to the calcination conditions: 8 h, 550°C and 8 h, 600°C (A) or 24 h, 450°C (C).

2.2. Physical-chemical characterization

Batches of the samples were analysed by various techniques, as indicated below. Surface areas were calculated from the amount of N_2 absorbed from a N_2–He stream, at liquid nitrogen temperature [5]. Pore volume and pore size distribution in the range from 75 to 75 000 Å were measured by a mercury-porosimeter (C. Erba model AG/60). Total pore volume was determined by the water titration method [6]. Particle size distribution was obtained microscopically by planimetric methods. Optical microscopy measurements were performed on a polarising Ortholux Leitz microscope, up to × 1200 magnification. High refractive indexes were determined using a universal stage by comparison with sulphur and selenium mixtures (Merwin mixtures) [7]. X-ray diffraction techniques were used to confirm the phase distribution.

3. Results

3.1. Phase distribution

Four optically distinct phases were found in the samples of the binary oxide system: MoO_3, TeO_2 (paratellurite), Te_2MoO_7 and an amorphous phase. The colourless MoO_3 crystallites are characterized by parallel extinction, marked idiomorphism, prismatic habit and exhibition of a network of cleavages. MoO_3 has refractive indices n_X(Li) = 2.09, n_Y(Li) = 2.26, n_Z(Li) = 2.36; the crystals are biaxial negative (−), $2V = -66°$. Partially reduced specimens are bluish, especially at the cleavages. Paratellurite crystals are prismatic, uniaxial positive (+), with $E = 2.36$ and $O = 2.24$. Te_2MoO_7 was found as pale-yellow spherulitic aggregates or as prismatic translucent crystals, often with random MoO_3 inclusions. The compound has refractive indices varying between 2.10 and 2.20 and lacks pleochroism. Optically isotropic (amorphous) material is present mainly as bright yellow conchoidal fragments, appearing dark under crossed nicols or showing anomalous polarization produced by strain within the crystal.

3.2. Morphological study

Loading of MoO_3 with TeO_2 causes drastic structural and textural changes in the solid through chemical reaction and incipient sintering phenomena; these effects are clearly illustrated by results of surface area (SA) and pore volume (V_p) measurements, as shown in Fig. 1 for samples calcined at 450°C (series C). Furthermore, optical microscopy indicates that the porosity of the original irregularly shaped grains of MoO_3 diminishes on addition of tellurium, leading to rather well-defined crystals when the composition Te_2MoO_7 is reached. This behaviour is in accordance with the results of the phase diagram, as qualitatively expressed by the liquidus curve (Fig. 2) [2].

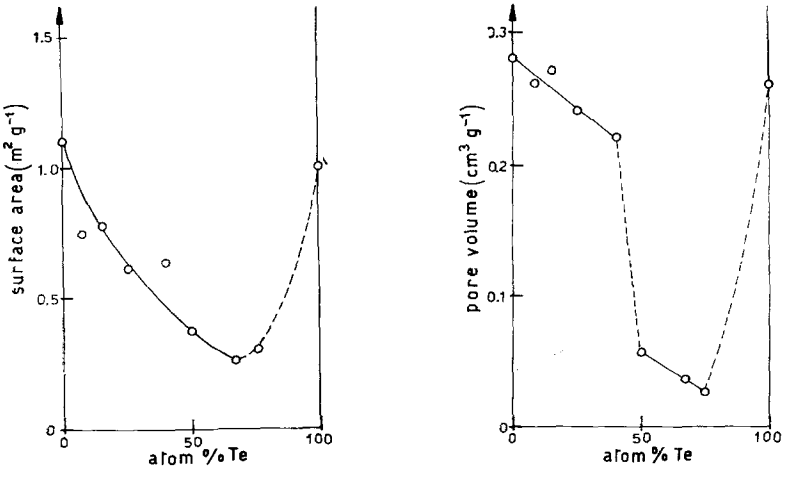

Figure 1 Surface areas and pore volumes of TeO_2–MoO_3 samples calcined at 450°C for 8 h (series C).

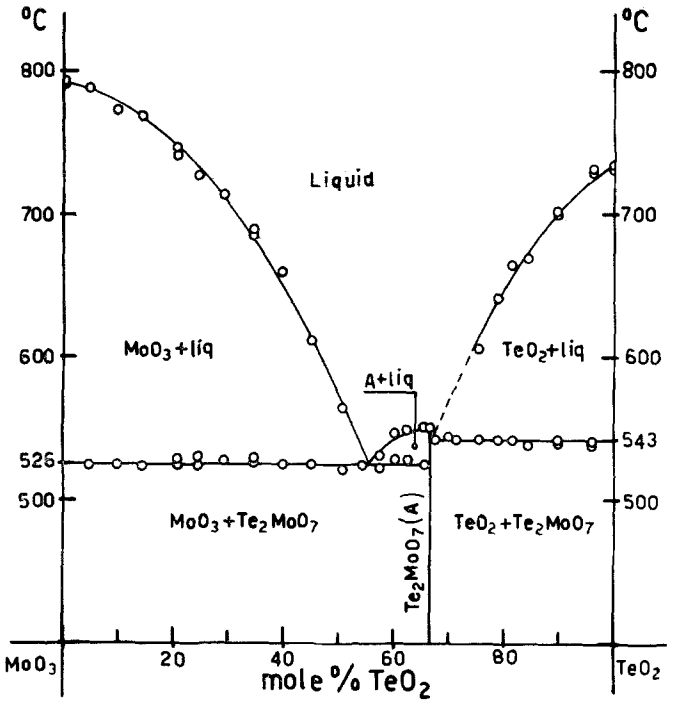

Figure 2 Phase diagram of the binary oxide system TeO_2–MoO_3.

Considering the various samples in the succession, we observe that the grain size of the MoO_3 crystallites diminishes with increasing tellurium content and depends upon the calcination conditions: higher activation temperatures (A-series) favour crystal-growth of the MoO_3 crystallites in otherwise amorphous samples. The yellow colour of the crushed grains of crystalline samples gradually brightens with increasing tellurium content. Calcination at higher temperature (600°C) imparts an even brighter yellow colour to the samples (A-series).

Optical examination of the sliced $Mo_{12}Te_1$/A-sample shows an open structure with polyhedral interparticle cavities and particles consisting of idiomorphic MoO_3 aggregates impregnated in correspondence to cleavages and cemented by a yellow optically isotropic mass (Figs. 3 and 4).

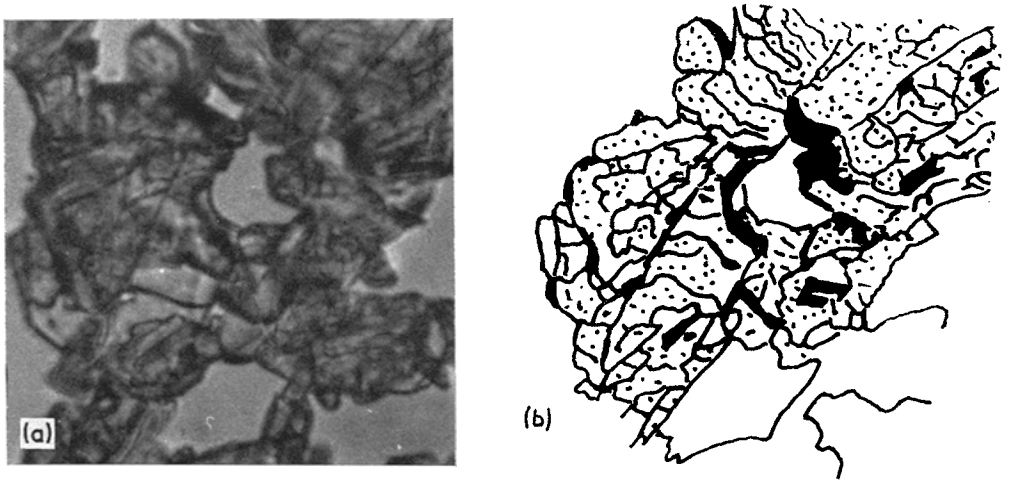

Figure 3 Microphotograph of the $Mo_{12}Te_1$/A samples; × 10^3. (a) Transparent light, (b) key: solid areas, mainly amorphous; dotted areas, MoO_3; open areas, cavity.

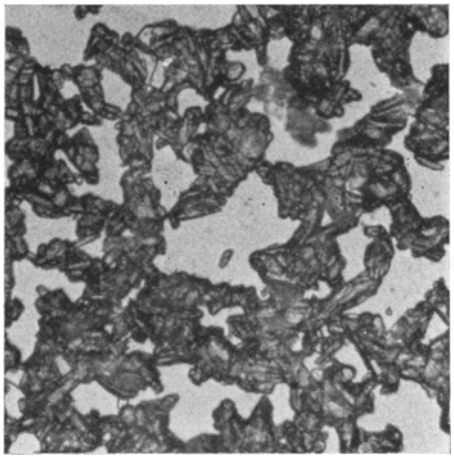

Figure 4 Microphotograph of the $Mo_{12}Te_1/A$ sample; × 350. Transparent light.

X-ray diffraction detects MoO_3 and indicates the presence of non-crystalline material which should contain tellurium. At higher tellurium contents, up to $Mo_{12}Te_4/A$, the structure is more compact, initially with worn polyhedral cavities, then well-rounded ones (Fig. 5); MoO_3 crystals exhibit a finer grain size.

Samples calcined at 450° C (C-series) consist of pseudocrystals built up of microcrystalline MoO_3 aggregates, cemented by an optically anisotropic yellow-coloured crystalline material, presumably Te_2MoO_7. Tellurium-poor specimens (< 20 mol % TeO_2) have an open structure with polyhedral cavities (Fig. 6a), whereas the grains of TeO_2 richer samples contain microspheroidal cavities, indicating large sintering effects (Fig. 6b). The interparticle cement forms aggregates

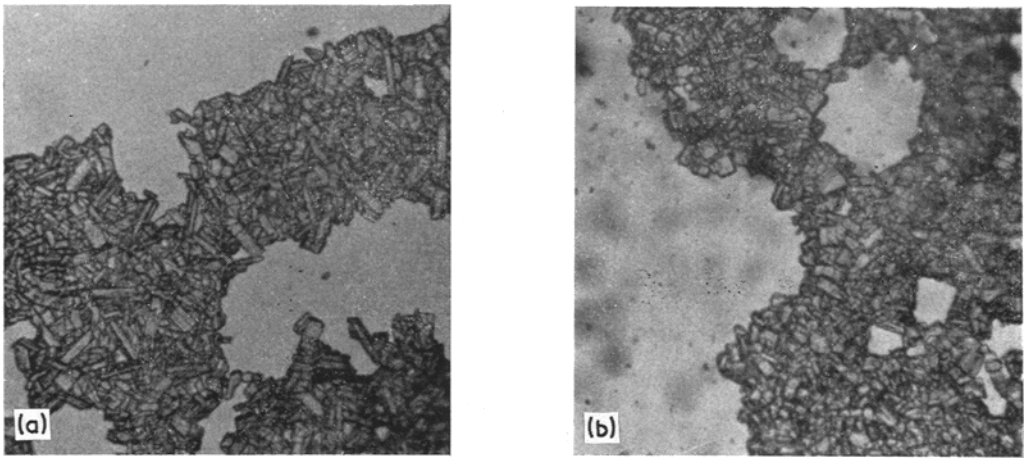

Figure 5 Microphotographs of the $Mo_{12}Te_2/A$ (a) and $Mo_{12}Te_4/A$ (b) samples; × 350. Transparent light.

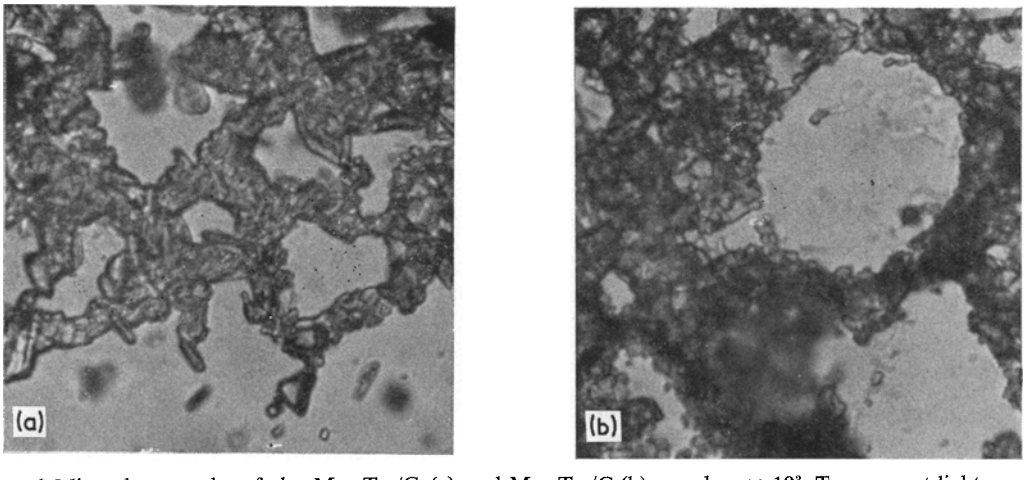

Figure 6 Microphotographs of the $Mo_{12}Te_2/C$ (a) and $Mo_{12}Te_4/C$ (b) samples; × 10^3. Transparent light.

of macrocrystals with poikiloblastic texture, containing inclusions of MoO_3. The Te_2MoO_7 ($Mo_{12}Te_{24}$) specimen is constituted of grains of vacuolar structure with polyhedral cavities. The kind of radial structure of the homogeneous mass points to recrystallization in the solid state (Fig. 7). In TeO_2 rich samples ($Mo_{12}Te_{36}$/C)

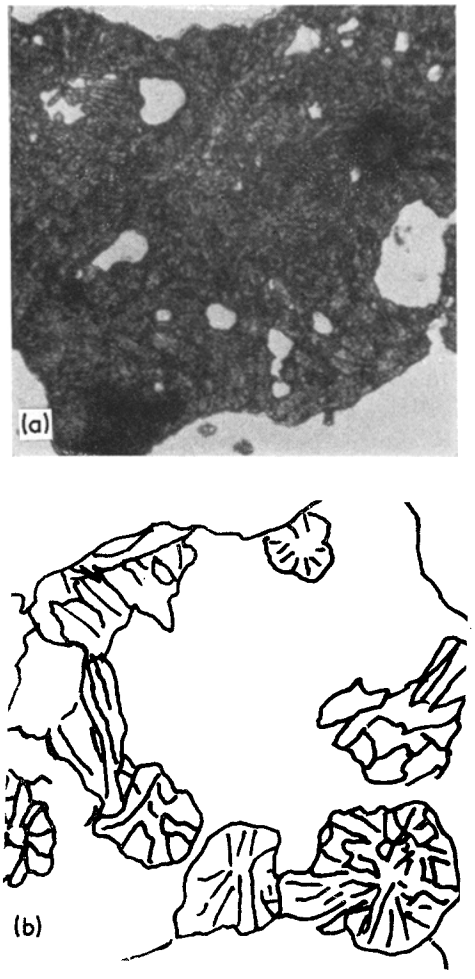

Figure 7 Microphotograph of the $Mo_{12}Te_{24}$/C sample; × 350. (a) Transparent light, (b) radial structure of the homogeneous mass.

crystallization also occurs radially and a second component (paratellurite) is present with a much finer grain size.

To provide more detailed information on the distribution of the various components of the system, intergranular embrittlement and brittle fracture due to oxygen depletion were observed during reduction experiments, carried out at room temperature with reducing agents consisting of either diluted $SnCl_2$/HCl and/or Zn/HCl solutions (the latter being the stronger). Chemical attack with the $SnCl_2$/HCl solution leads to disgregation of the agglomerates, with ultimate particle size distributions as shown in Fig. 8a. Optical microscopy clearly shows accumulation of reduced fines and dusky powder on top of the MoO_3 grains. Comparison with samples before reduction indicates no significant modifications with respect to the original grain size of MoO_3, at least up to $Mo_{12}Te_8$/C; at this composition, a bimodal particle size distribution is observed which chemical analysis helps to attribute to reduced Te_2MoO_7 and "MoO_3". Further, by creating an appropriate redox gradient in a solvent it became possible to segregate mechanically the binary compound from the MoO_3 matrix (Fig. 10). Samples of $Mo_{12}Te_{24}$/C and those containing excess of TeO_2 degrade slowly into a solid with finer grain size distribution, differing considerably from the original samples. Higher resistance to disintegration of tellurium-rich samples clearly reflects larger sintering effects in this region (Fig. 1).

Comparison of particle size distributions as a result of previous treatment (Fig. 8a) and of successive attack with Zn/HCl (Fig. 8b) shows no differences in the unimodal grain size distribution for samples up to $Mo_{12}Te_4$/C. In contrast, the bimodal distribution found in the $Mo_{12}Te_8$/C sample changes the mean diameters from Φ = 2.2 and 0.75 μm after attack with the weakest reducing agent into Φ = 2.2 and 0.58 μm after leaching with the stronger reductant. Similar measurements for $Mo_{12}Te_{24}$/C following mild and strong reduction lead to unimodal distributions with Φ = 0.70 and 0.50 μm respectively. It thus appears that the second attack diminishes the mean diameter of the grains of the cementing agent.

As to the $Mo_{12}Te_x$/A series, results of reduction experiments are shown in Fig. 9a and b respectively for the first ($SnCl_2$/HCl) and after the successive attack by Zn/HCl. Large differences are evident in the case of $Mo_{12}Te_1$ and $Mo_{12}Te_2$, as much finer grain sizes are found after the strongest attack.

4. Discussion

The results reported above evidentiate that addition of TeO_2 favours agglomeration of

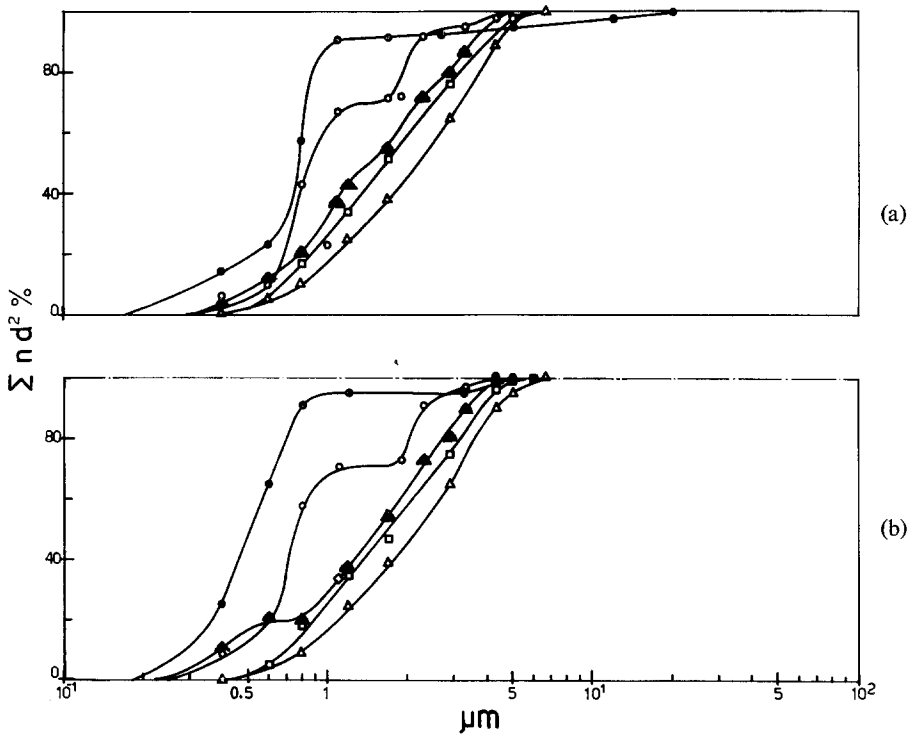

Figure 8 Particle size distribution of samples after reduction with $SnCl_2$/HCl (a) and successive attack by Zn/HCl (b); △ $Mo_{12}Te_1$/C, □ $Mo_{12}Te_2$/C, ▲ $Mo_{12}Te_4$/C, ○ $Mo_{12}Te_8$/C, ● $Mo_{12}Te_{24}$/C.

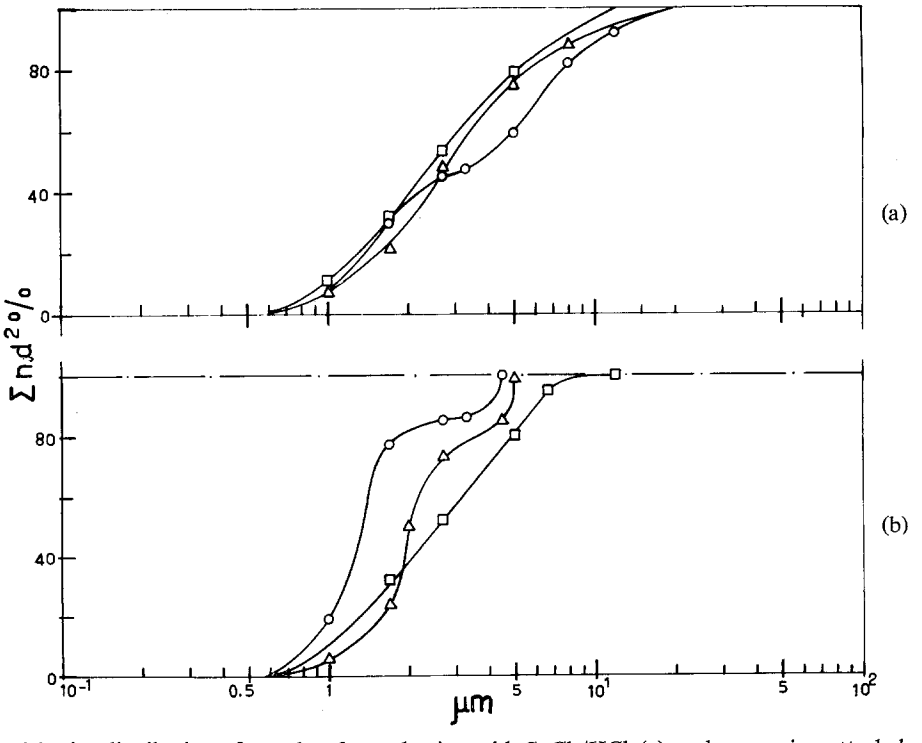

Figure 9 Particle size distribution of samples after reduction with $SnCl_2$/HCl (a) and successive attack by Zn/HCl (b); △ $Mo_{12}Te_1$/A, ○ $Mo_{12}Te_2$/A, □ $Mo_{12}Te_4$/A.

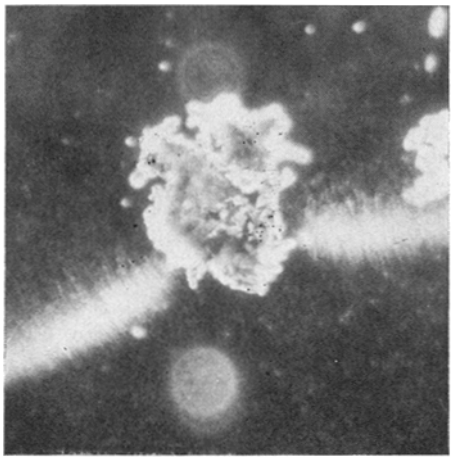

Figure 10 Dark-field microphotograph of a grain of a binary oxide mixture MoO_3–TeO_2 under the action of a reducing front.

MoO_3 crystals. This effect occurs via formation of an amorphous or crystalline Te–Mo binary oxide, capable of permeation through large interparticle spaces and cementing the MoO_3 crystallites (Figs. 3 to 7).

The idiomorphism of MoO_3 grains contrasts to the allotriomorphic character of Te_2MoO_7; the coverage of the MoO_3 crystals with the binary oxide is thus rationalized. The role of the binary oxide as interparticle ligand is also consistent with the chemical interaction concepts discussed elsewhere [1], considering that the binary mixtures have lower melting points (Te_2MoO_7 m.p. = 551°C, eutectics at 526 and 543°C) and as a consequence TeO_2-loaded MoO_3 has a "lower" viscosity than MoO_3, with higher mobility of the solid. Owing to this, Te_2MoO_7 permeates through the mass causing fragmentation of the original grains of MoO_3 down to a finer grain size, as the TeO_2 content is increased. On the macroscopic scale, volume migration manifests itself in TeO_2-loaded MoO_3 by the agglomeration of the particles into more ordered and compact structures, with disappearance of interparticle cavities. The coalescence of elementary particles to form more compact ones is reflected in the pore volume and surface area values which drop rapidly with increasing tellurium contents, reaching minimum values between 50 and 80 mol % TeO_2 for samples calcined at 450° C (Fig. 1). This behaviour is in accordance with the expectation based on the phase diagram (Fig. 2) namely, the lowest melting points are comprised in this region with an absolute minimum (526°C) in correspondence with the eutectic of Te_2MoO_7 and MoO_3 (55 mol % TeO_2). Thus loading of MoO_3 with TeO_2 results in an increase of low melting components and thus favours sintering phenomena, as is demonstrated by the variations in surface area and pore volumes; this is also common to the supported systems.

Reduction experiments performed at room temperature and followed by means of microphotography give evidence for a larger variation in intergranular strength as a function of TeO_2 content. MoO_3 crystals which do not disintegrate in a $SnCl_2$/HCl solution contrast to TeO_2 loaded samples, confirming the cementing function of Te_2MoO_7. The grain size distribution after attack by reducing agents (Figs. 8a and b, 9 a and b) confirms qualitatively the observations concerning the dependence of the grain size of MoO_3 upon composition and preparative route. It further shows clearly that MoO_3 influences the reducibility of the binary oxide. In samples in which a binary oxide layer covers crack-free MoO_3 grains, as in $Mo_{12}Te_1$–$Mo_{12}Te_4$/C (Fig. 6) and $Mo_{12}Te_4$/A (Fig. 5), the grain size distribution of MoO_3 after reduction is quite independent on the strength of the reducing agent (Figs. 8 and 9). Other samples, usually those consisting of irregular and fractured grains, as $Mo_{12}Te_1$–$Mo_{12}Te_2$/A (Fig. 4), have a different behaviour (see below). The difference is understood by considering Fig. 11, which shows a sliced section of a $Mo_{12}Te_1$/A sample in a Merwin mixture [7]: by this means, it was possible to show Te_2MoO_7 deposition on

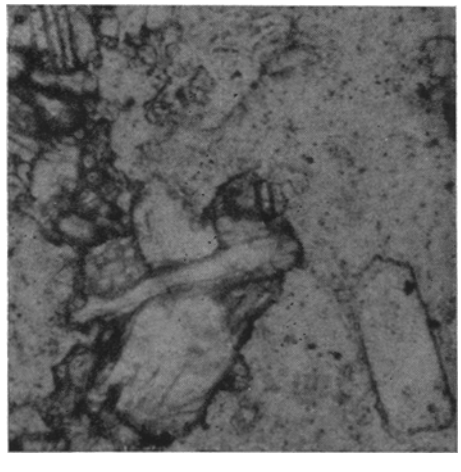

Figure 11 Microphotograph of a sliced section of the $Mo_{12}Te_1$/A sample in a Merwin mixture; × 10^3.

continuous internal surfaces, and thus loci of high embrittling element concentration and preferred fracture paths in the crystals. In these cases the grain size varies with the strength of the reducing agent (Fig. 9a and b), as a stronger medium leads to cracking of MoO_3 grains along less accessible permeated fractures. These findings are to be compared with the fine grain size of the pure $Mo_{12}Te_{24}$ (Te_2MoO_7) sample (Fig. 8a and b) after chemical treatment, which varies with the reducing power of the reagent and depends on the chemical nature of the compound. On the other hand, in view of the high mobility of the low melting solid, physical factors, such as the presence of imperfections in crystals, are not expected to play a role in providing numerous sites for chemical attack. The slow rate of disintegration by reduction of samples with a high TeO_2 content is explained by their compact structure.

The cementing function of Te_2MoO_7, i.e. the coverage of MoO_3 particles by the binary compound appears to provide a reasonable explanation for the observed trend in the catalytic properties. The system described represents some typical features of "adlineation" promotion in catalysis, as illustrated in Fig. 12

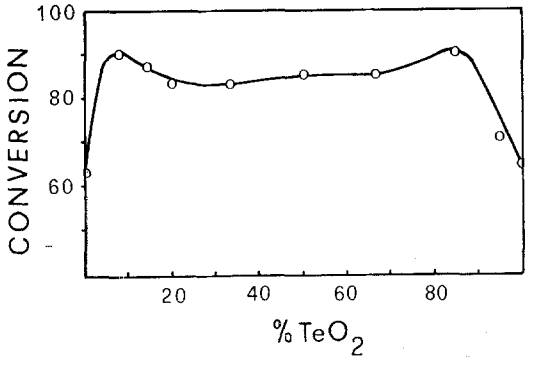

Figure 12 Conversion (in %) of propylene in the ammoxidation reaction over TeO_2–MoO_3/75% SiO_2 catalysts at 440° C as a function of the mol % TeO_2.

for the conversion of propylene at 440° C in the ammoxidation reaction, using catalysts consisting of 25% active phase (Te–Mo oxides) supported on microspheroidal SiO_2 [8]. Thus, following the observations for the isolated system TeO_2–MoO_3, the promoting effect of small amounts of TeO_2 may derive from the high fraction of surface Te_2MoO_7, a compound which is more reducible than MoO_3.

5. Conclusions

Loading of MoO_3 with TeO_2 causes drastic changes in morphology (porosity, structure, texture and surface topology) of the solid depending upon the activation conditions and composition. The morphological properties of the MoO_3–TeO_2 system closely follow the chemical interactions occurring in the system, in accordance with the phase diagram, and vary more drastically for silica supported samples than for the binary oxide mixtures. Experimental evidence supports a model for binary oxide samples consisting of impregnated MoO_3 aggregates cemented by an intergranular Te_2MoO_7 surface. Reduction at room temperature leads to intergranular embrittlement due to oxygen depletion at grain boundaries and brittle fracture of MoO_3 crystallites in correspondence to second phase deposition (Te_2MoO_7) on the internal surfaces. The equilibrium grain size distribution varies with the reducing agent and time, as well as with the composition and morphological properties of the sample. This holds both for mixed oxide compositions and Te_2MoO_7, thus excluding that the effects of the reducing agent may simply be attributed to dissolution of the cementing material.

References

1. J. C. J. BART, G. PETRINI and N. GIORDANO, *Z. Anorg. Allg. Chem.* (in press).
2. G. PETRINI, J. C. J. BART, P. PERISSINOTO and N. GIORDANO, Proceedings of the 4th ICTA, Budapest, 8-13 July, 1974.
3. N. GIORDANO and G. CAPORALI, Congrès Intern. du Cinquantenaire Soc. Chim. Industr., Paris, 24-31 May, 1968.
4. V. N. ZHIZNEVSKII, E. V. FEDEVICH, O. M. PIKULYK, V. YA. SHIPAILO and D. K. TOLOPKO, *Kinet. i. Kataliz* **13** (1972) 1488.
5. F. M. NELSEN and F. T. EGGERTSEN, *Anal. Chem.* **30** (1958) 1387.
6. AMERICAN PETROLEUM INSTITUTE, "Physical Properties of Cracking Catalysts: A Progress Report" (1959) p. 37.
7. H. E. MERWIN and E. S. LARSEN, *Amer. J. Sci.* **34** (1912) 42.
8. G. CAPORALI, N. FERLAZZO and N. GIORDANO (to Montecatini-Edison), U.S. Pat. 3,691,224 (12 September, 1972).

Received 28 August and accepted 20 November 1974.